HHS Public Access

Author manuscript

Osteoporos Int. Author manuscript; available in PMC 2022 November 01.

Published in final edited form as:

Osteoporos Int. 2021 November ; 32(11): 2335–2346. doi:10.1007/s00198-021-06006-1.

Bone biomechanical properties and tissue-scale bone quality in a genetic mouse model of familial dysautonomia

Ghazal Vahidi[a], **Hannah Flook**[a], **Vanessa Sherk**[b], **Marc Mergy**[c], **Frances Lefcort**[c], **Chelsea M. Heveran**[a,†]

[a]Department of Mechanical & Industrial Engineering, Montana State University, USA,

[b]Department of Orthopaedics, University of Colorado School of Medicine, USA

[c]Department of Microbiology & Immunology, Montana State University, USA

Abstract

Purpose: Familial dysautonomia (FD) is associated with a high prevalence of bone fractures, but the impacts of the disease on bone mass and quality are unclear. The purpose of this study was to evaluate tissue- through whole-bone scale bone quality in a mouse model of FD.

Methods: Femurs from mature adult *Tuba1a-Cre; Elp1*$^{LoxP/LoxP}$ conditional knockouts (CKO) (F = 7, M = 4) and controls (F = 5, M = 6) were evaluated for whole bone flexural material properties, trabecular microarchitecture and cortical geometry, and areal bone mineral density (BMD). Adjacent maps spanning the thickness of femur midshaft cortical bone assessed tissue-scale modulus (nanoindentation), and bone mineralization, mineral maturity, and collagen secondary structure (Raman spectroscopy).

Results: Consistent with prior studies on this mouse model, the *Elp1* CKO mouse model recapitulated several key hallmarks of human FD, with one difference being the male mice tended to have a more severe phenotype than females. Deletion of *Elp1* in neurons (using the neuronal-specific *Tuba1a-cre*) led to a significantly reduced whole-bone toughness but not strength or modulus. Elp1 CKO female mice had reduced trabecular microarchitecture (BV/TV, Tb.Th, Conn.D.) but not cortical geometry. The mutant mice also had a small but significant reduction in cortical bone nanoindentation modulus. While bone tissue mineralization and mineral maturity were not impaired, FD mice may have altered collagen secondary structure. Changes in collagen secondary structure were inversely correlated with bone toughness. BMD from dual-energy x-ray absorptiometry (DXA) was unchanged with FD.

Conclusion: The deletion of *Elp1* in neurons is sufficient to generate a mouse line which demonstrates loss of whole bone toughness, consistent with the poor bone quality suspected in the clinical setting. The Elp1 CKO model, as with human FD, impacts the nervous system, gut, kidney

†Corresponding Author, T +1 406-994-2010, chelsea.heveran@montana.edu.

Conflict of interest: All authors declare that they do not have conflicts of interest.

function, mobility, gait, and posture. The bone quality phenotype of Elp1 CKO mice, which includes altered microarchitecture and tissue-scale material properties, is complex and likely influenced by these multi-systemic changes. This mouse model may provide a useful platform to not only investigate the mechanisms responsible for bone fragility in FD, but also a powerful model system with which to evaluate potential therapeutic interventions for bone fragility in FD patients.

Keywords

Familial dysautonomia; bone toughness; bone quality

1.0 Introduction

Familial dysautonomia (FD) (also known as Riley-Day Syndrome) is a rare hereditary neurodevelopmental and neurodegenerative disease, affecting Jewish populations of Ashkenazi descent.[1] FD is caused by a mutation in the gene *ELP1* (previously referred to as *IKBKAP*), which results in mis-splicing of the pre-mRNA that encodes the ELP1 (formerly Ikap) protein.[1–4] Different cell types exhibit varying capacity to splice the mutant mRNA.[5,6] Since neurons are the least capable of splicing the mutated mRNA, ELP1 reduction primarily affects the peripheral and central nervous systems, [5–8] and especially sensory and autonomic fibers.[9,10] In addition to other physical impairments affecting sensory,[11] digestive,[12] respiratory,[13] and cardiac systems,[11] FD is clinically associated with several musculoskeletal issues, such as gait disorders, foot and spinal deformities, and bone fragility. Up to 60% of FD patients experience one or more fractures during their lifetime.[14] There is not an accepted treatment plan for bone fragility in FD,[15] in part because the reasons for bone fragility in this vulnerable population are not understood. Bone fracture resistance is determined by bone mass and bone quality.[16,17] The limited clinical data pertaining to bone in FD patients indicates that patients with FD have lower bone mineral density as measured by dual-energy x-ray absorptiometry (DXA) as well as decreased serum markers of bone formation and increased markers of bone resorption.[18] Bone quality may also be reduced in FD. This population commonly suffers from spinal deformities and vertebral fractures, and spinal fixation operations are often needed.[19–21] Spinal fixation failure (e.g., hook and screw pullout) is common in FD patients, suggesting that FD may reduce bone quality (i.e., bone tissue material properties and microarchitecture). FD deleteriously impacts nutrient absorption,[22] kidney function, [23] posture, and gait,[19] which may all contribute to bone quality defects.

FD is a rare disease and the opportunity to collect human samples is extremely limited. A mouse model of FD offers new directions for investigating the impacts of this disease on bone mass and bone quality. Our model was developed through crossing *Tuba1a-Cre* mice (C57Bl/6 background) in which the *Cre* targets neurons in both the peripheral nervous system (PNS) and central nervous system (CNS), with floxed *Elp1* mice to generate *Tuba1a-Cre; Elp1*$^{LoxP/LoxP}$ conditional knockouts.[8] The *Elp1* gene is located on chromosome 4 in the mouse, which is an analogous region to human chromosome 9q31.3.[24] The mouse ELP1 protein has 80% amino acid similarity with human ELP1.[20,25] This genetic model has already revealed a role for *Elp1* in the developing and adult CNS and PNS.

[5,8,26] Ablation of *Elp1* in the nervous system alone can recapitulate many human FD hallmarks such as kyphoscoliosis and degeneration of the sympathetic and sensory nervous systems, severe reduction in nociceptive neuronal numbers, poor locomotor coordination, unsteady gait and postural instability, and gastrointestinal dysfunction.[8,27] The phenotype severity is related to decline in amount of *Elp1*.[20] Our model is one of only two current models that survive to adulthood.[8,27–29] Other Elp1 conditional knockout lines have been generated but do not survive beyond 24 hours after birth.[30–32] Bone quality has not been reported in this or any other FD mouse model.

The purpose of this study was to investigate whether the Elp1 CKO mouse model impairs bone mass and multiscale bone quality. At the whole-bone scale, we evaluated bone toughness, strength, and modulus. At the tissue scale, we evaluated bone microarchitecture, modulus, mineralization, and biomarkers of collagen secondary structure. We hypothesized that our FD mouse model would have reduced whole-bone toughness as well as reduced tissue-scale bone quality.

2.0 Materials and Methods

2.1 Animal model

All mouse studies were approved by the Institutional Animal Care and Use Committee at Montana State University. To generate *Elp1* conditional knockouts (CKO), floxed *Elp1* mice were crossed with *TUBA1a* promoter-driven *Cre* (*Tα1-Cre*) mice, which targets postmitotic neurons. Mice that were Cre-negative but contained the same floxed *Elp1* exon as the mutants, were used as controls. Female and male *Tuba1a-Cre; Elp1*$^{LoxP/LoxP}$ mutants (F = 7, M = 4) and controls (F = 5, M = 6) were housed in phenotype groups and fed standard mouse chow. At ages 7–10 months, mice were evaluated for disease severity with a phenotype classification system (Supplementary Table 1). The scoring matrix consists of 8 criteria. Mice were scored for the presence or absence of a particular phenotype or on a scale of 1–2 with regard to severity, with a maximum score of 12. For this assessment, weight was assessed qualitatively. Weight was also quantified in a separate exam (Table 1). This FD phenotype was previously characterized in detail by Chaverra *et al*.[8] Animals were euthanized by isoflurane followed by cervical dislocation at an age of 7–10 months, based on mouse health and necessity for other studies. Femurs were collected immediately after euthanasia.

Femurs were harvested and frozen at −20° C in phosphate-buffered saline-dampened gauze prior to analysis. Femurs underwent three-point bending (Instron 5543, 1 kN load cell) to quantify whole-bone material properties. Femurs were tested to failure at a rate of 5 mm/min on a custom anvil with 8 mm span, with care taken to maintain their hydration. Following testing, the femoral diaphysis at the location of fracture was imaged with scanning electron microscopy (SEM; Zeiss Supra 55VP, WD = 8 mm, accelerating voltage = 10 kV) in variable pressure mode. Using I_{ML} and C_y measured from SEM images, load-displacement curves were analyzed for modulus, ultimate stress, and toughness using standard beam bending equations as applied to the mouse femur.[33] Following whole-bone mechanical testing, femurs were histologically dehydrated in a graded series of ethanol and embedded in poly(methyl)methacrylate (PMMA) for further analyses.[34]

2.2 Trabecular microarchitecture and cortical geometry

The trabecular bone microarchitecture of the distal femur metaphysis was assessed using microCT of PMMA-embedded femurs for all study mice (μCT, Scanco 80, 55 kVP, 114 mA, integration time 900 ms). Scanning was performed with 10 μm voxel size. The metaphysis volume of interest was defined as the 100 slices proximal from the end of the growth plate. Trabecular regions were designated on each two-dimensional transverse slice using hand-drawn contours that excluded the cortical shell. Trabecular parameters included trabecular number (Tb.N), trabecular spacing (Tb.Sp), trabecular thickness (Tb.Th), mineralized bone volume (BV), total bone volume (TV), bone volume fraction (BV/TV), trabecular connectivity density (Conn.D), and structure model index (SMI). Cortical geometry parameters included cortical area (Ct.Ar), the minimum moment of inertia (I_{min}) and cortical thickness (Ct.Th).[35]

2.3 Tissue-scale modulus from nanoindentation

PMMA-embedded femurs were sectioned at the mid-diaphysis using a low speed diamond saw (Isomet, Buehler), and then were polished with wet 600 and 1000 grit silicon carbide papers (Buehler), followed by alumina suspensions (9, 5, 3, 1, 0.5, 0.3, and 0.05 μm) to achieve a mirror finish. Samples were sonicated in tap water between each step to remove remaining alumina particles.

Nanoindentation (KLA Tencor iMicro, Milpitas, CA) was performed at the posterior-lateral quadrant in maps spanning the cortical thickness to be consistent with tissue-scale analyses in other recent investigations of bone diseases and aging (Figure 1).[36,37] Four indents per row were placed in arrays extending through the cortical thickness (spacing 15 μm in x and y). Samples were indented with a Berkovich tip at 30 nm/s velocity until a target load of 5 mN was achieved. A 60s hold at the peak load was incorporated to allow viscoelastic energy to dissipate before the unloading.[38] The modulus was calculated using the Oliver Pharr approach.[39] Briefly, the 95^{th}-45^{th} percentile of the unloading curve was fit with a second-order polynomial.[40] A tangent line at the start of this section was used to calculate the stiffness, S. The tip contact area, calculated as a function of contact depth from calibration on fused silica and S were used to calculate the reduced modulus, E_r (Equation 1). Then, using the known tip modulus and Poisson's ratio (1140 GPa and 0.07, respectively), the indentation modulus E_i was calculated from E_r (Equation 2).

$$E_r = \frac{S}{2}\sqrt{\frac{\pi}{A}} \quad \text{(Equation 1)}$$

where E_r is the reduced modulus, S is the initial unloading stiffness (the slope of the unloading curve evaluated at the maximum load, $\frac{dP}{dh}$), and A is the projected contact area between the indenter tip and the sample at maximum load.

$$\frac{1}{E_r} = \frac{1-\upsilon_i^2}{E_i} + \frac{1-\upsilon_t^2}{E_t} \quad \text{(Equation 2)}$$

where subscript i refers to the substrate material, subscript t refers to the tip material, and υ is Poisson's ratio.

2.4 Tissue-scale bone composition from Raman spectroscopy and Dual-Energy X-ray Absorptiometry

Raman spectroscopy was performed in maps spanning the cortical thickness adjacent to the nanoindentation arrays. Raman spectra were collected in rows of three spots spaced 15 μm apart extended every 15 μm through the cortical thickness (Figure 1). A Horiba Confocal microscopy system (Horiba LabRam) was used with a 785 nm wavelength laser and a 50× objective (NA 0.75). A 5^{th} order polynomial was fitted to data to subtract the fluorescent baseline. A reference PMMA spectrum was subtracted from each point using a custom MATLAB code. These corrected spectra were then analyzed for area ratios of mineral:matrix (ν_2 phosphate:amide III), carbonate:phosphate, crystallinity (inverse of half-width at full maximum height of the ν_1 phosphate peak), and plastic:phosphate (Figure 1). Points with greater than 50% plastic:phosphate were excluded from analysis. The amide I envelope was assessed for changes in the collagen secondary structure using the intensity ratios I1670:I1640, I1670:1690, and I1670:1610, consistent with the methods of Unal *et al.*[41]

Areal bone mineral density (BMD) of PMMA-embedded distal femurs was measured by Dual-Energy X-ray Absorptiometry (DXA) (Faxitron Bioptics, Tucson, AZ) at the metaphysis.

2.5 Statistical analyses

To avoid overpowered analyses, nanoindentation and Raman measurements were averaged per measure per mouse such that one mean and one standard deviation for each measure were input into statistical models. The main effects of sex, FD, and the interaction of sex and FD, were assessed on all bone outcomes using ANOVA (Minitab, v18). Dependent variables were transformed, if necessary, such that all models satisfied assumptions of residual normality and homoscedasticity. Significance for main effects was set a priori to $p < 0.05$. Significant interactions between FD and sex were followed up with post-hoc tests. Care was taken to maintain family-wise type I error at 0.05 through a Bonferroni correction. For most measures, FD vs control was compared for females and males (i.e., two comparisons, critical α: 0.05/2 = 0.025). Because some variations in bone mechanical properties and microarchitecture is expected between 7–10 months of age,[42,43] all measures except for disease severity scores were run with age as a covariate in additional ANCOVA analyses. This was to confirm that observed changes in the bone properties were because of the FD and sex, and not trivially explained by differences in the age. To test Likert-like disease severity scores between female and male FD mice, a two sample t test was performed to compare the data, which were normally distributed.[44–46]

3.0 Results

All measures evaluated with 2-factor ANOVA (i.e., all measures except disease severity) were first assessed with age as a covariate. All factors for which there was a significant

effect of FD, sex, or an interaction between FD and sex continued to be significant when including age as a covariate. Therefore, we report the results of 2-factor ANOVA without the covariate.

3.1 Disease severity in response to conditional Elp1 knockout

Both male and female *Elp1*conditional knockout mice (referred to hereafter as 'FD') varied in phenotypic severity and body size (Table 1). FD and sex had an interactive effect such that males had a more severe FD phenotype than females. Similarly, FD and sex had an interactive effect on mouse body mass measured at euthanasia. FD males were significantly smaller than control males ($p = 0.003$, −18.3%). However, FD females were not smaller than control females. FD females with more severe FD scores had smaller body mass (Spearman's $\rho = -0.818$, $p = 0.024$). There was not a significant correlation between body mass and FD severity for males, although the range of both variables were smaller than for females. FD females displayed mean and median disease severity of 3.9 and 4, respectively, with a range of 2 to 6. FD males displayed mean and median disease severity of 6.3 and 6.5, respectively, with a range of 5 to 7. Males had higher disease severity scores compared to females ($p=0.014$). Females had slightly longer femurs than males ($p = 0.009$, +3.3%) but FD did not affect the femur length.

3.2 Trabecular microarchitecture and cortical geometry

There were significant interactions between FD and sex for several measures of trabecular microarchitecture, including BV, BV/TV, Conn.D., and SMI (Table 2). FD reduced BV/TV for females (−55.4%, $p = 0.001$) but not for males, which was in good correspondence with a similar decrease in BV for female mutants compared with controls. FD reduced Conn.D in females (−78.2%, $p = 0.006$) but this measure increased in males (+75.2%, $p = 0.015$). SMI in female mice increased with FD to be more rod-like compared to controls (+32.2%, $p = 0.002$) but not for males. Other measures did not show interactions and thus we interpret the main effects of FD and sex. Tb.Th decreased with FD as a main effect (−16.1%, $p = 0.020$). Other measures of trabecular microarchitecture (Tb.Sp and Tb.N) showed expected effects of sex [47] but were not affected by FD. As expected, [48] females had smaller Ct.Ar and I_{min} than males, although Ct.Th was not different among groups. However, there were no differences in cortical geometry with FD status.

3.3 Whole-bone flexural properties

Work to fracture was lower with FD (−31.9%, $p=0.004$) in both males and females. Toughness, the geometry-independent analogue of work to fracture, was also lower with FD (−36.76%, $p=0.001$) in both sexes. Toughness was not significantly correlated with disease severity ($p > 0.05$). When accounting for the cross-sectional geometry of the specimens, geometry-independent modulus and strength were not affected by sex nor FD.

3.5 Tissue-scale material and mechanical properties

We employed nanoindentation and Raman spectroscopy to evaluate the effect of FD on tissue-scale modulus and composition (Table 4). Mean nanoindentation modulus (E_i) decreased with FD (−4.4%, $p=0.041$). Standard deviation of E_i was unaffected by FD

or sex. All measures of tissue-scale bone composition from Raman spectroscopy were not significantly affected by either FD or sex. To investigate whether collagen secondary structure is affected by FD, we further analyzed the amide I peak from Raman spectroscopy using the intensity ratios I1670:I640, I1670:I1690, and I1670:I1610. There was a significant interaction of FD and sex on the I1670:I1640 ratio such that male FD mice had 27.3% higher values than male controls ($p = 0.005$). I1670:I1690 was significantly higher for male sex and FD ($p < 0.05$ for both). The I1670:I1610 ratio was not significantly affected by either FD or sex. FD status did not affect the BMD from DXA scans of the distal femora, which is primarily trabecular bone. Females had lower BMD than males ($p=0.006$), consistent with their lower BV/TV values.[49–52]

4.0 Discussion

We present the first investigation of bone quality in a mouse model of FD. We observed similarities of this mouse model skeletal phenotype to human FD, including kyphoscoliosis and altered gait. However, unlike human FD, we did not observe decreased skeletal size (e.g., length of femur).[18,53] Both females and males showed variation in FD severity. FD was more severe for males, but more variable for females (Table 1). The increased disease severity in males is consistent with prior publications on this model but the mechanisms driving this difference in mice is not known.[8,27] However, the systems that have previously been examined in this model, including target innervation, neuronal survival and gastrointestinal system function have not revealed any differences by mouse sex.[8,27] Patients with FD have a well-described yet highly variable phenotype.[54] The mechanisms underlying this variation are not understood.[2,5,29] It has been suggested that this variation most likely reflects either the action of a genetic modifier and/or variation in translation of the *Elp1* mRNA.[5,29] In human patients with FD, there is no difference in clinical phenotype between males and females, hence it is likely that the variation between male and female mice is not an Elp1-related consequence.[5,55]

Fracture resistance is determined by bone mass and bone quality.[16,17] We therefore investigated the effect of FD on bone mass, tissue- through whole-bone scale material properties, and microarchitecture. Bone mineral density (BMD) from DXA was not impacted by FD. Conversely, FD impacted bone quality at multiple length-scales. At the whole-bone scale, FD reduced bone toughness but not bone strength. At the tissue-scale, FD resulted in a small but significant reduction in nanoindentation modulus. FD did not alter mineral:matrix or mineral maturity, but may impact the quality of the bone matrix. FD mice had higher I1670:I1690 ratio, which indicates matrix maturity.[56] The I1670:I1640 ratio, which indicates collagen secondary structure damage, was higher in FD males than controls. In previous reports, the I1670:I1640 ratio was negatively correlated with bone toughness.[41,57,58] In our study, toughness and I1670:I1640 were modestly correlated for all mice (Spearman's $\rho = -0.465$). When considering only males, which had the greatest range in both measures, the correlation improved ($\rho = -0.697$). Importantly, previous investigations of the relationships between amide I intensity ratios and bone toughness studied fresh bone and we studied PMMA-embedded and polished bone.[41,56–58] Thus, these altered amide subpeak ratios in FD could either relate to reduced bone matrix quality *in vivo*, to greater susceptibility of these bones to damage during embedding or polishing, or a combination

of these effects. In addition to collagen secondary structure,[56,58] other aspects of bone matrix quality (e.g., collagen crosslinking[59–61] and collagen-mineral interactions[62,63]) are found to influence bone fracture resistance in other disease models. Further evaluation of bone matrix quality is expected to be valuable for understanding bone fragility in FD.

Bone toughness and tissue-scale bone quality were reduced with FD in our mouse model, but these measures did not correlate with disease severity. This lack of correlation may reflect the multifactorial nature of the mouse FD phenotype. Human FD is also multifactorial. The impacts of human FD on bone quality could be caused by a combination of health conditions, including diet restrictions, reduced calorie intake, gut disfunctions and gastrointestinal tract malfunction,[2,22,23,64,65] antacid treatment,[18] kidney dysfunction, [23,66] decreased mobility and weight bearing activities,[19] and altered gait and posture. [67] These effects may individually or together impair bone quality during development and after skeletal maturity in FD. It is not clear if the lack of correlation between toughness and disease severity would extend to human FD.

Many of these confounding physiological conditions that occur alongside FD have the potential to alter bone mineral homeostasis. Our mouse model has commonalities with diseases that impair mineral homeostasis and promote high bone turnover, including decreased trabecular microarchitecture and decreased tissue-scale modulus.[34,68] However, we do not observe changes to bone mineralization or mineral maturity, which would usually be expected with altered bone turnover.[69–71] Further investigation (e.g., dynamic histomorphometry) is needed to identify whether bone turnover is altered in this mouse model.

Our model of FD affected some aspects of bone quality differently for males and females (Figure 2), which was observed as significant interactions between FD and sex. Higher I1670:I1640 was observed for males but not females. FD resulted in a dramatic loss of cancellous bone volume and connectivity for females but not for males. FD also dramatically decreased bone connectivity for females but significantly improved bone connectivity for males. It is possible that decreased total volume but similar trabecular number and thickness for FD males contributes to their large increase in Conn.D. However, the change in total volume is much smaller that the increase in bone connectivity, so it is possible that the increase in Conn.D. has other contributing factors. A large sample size, especially in males, would be valuable for understanding sex differences in this mouse model.

Bone is innervated with nerve fibers,[72,73] and bone remodeling depends on inputs from the central and peripheral nervous system.[74] Because FD primarily impairs the nervous system, an intriguing question is whether impaired nervous system function directly impacts bone quality as opposed to an indirect effect through other organs (e.g. kidney and gut) or through altered posture, gait, and loading. FD patients suffer from a loss of calcitonin gene-related peptide, which is the primary neurotransmitter in unmyelinated neurons and extensively distributed in the CNS and PNS.[75–77] In a study on Sprague-Dawley rats without any genetic alterations, it was reported that capsaicin-sensitive sensory neurons -which are mostly unmyelinated neurons and some small myelinated neurons- contribute to

the maintenance of trabecular bone integrity, since lesioning of the unmyelinated sensory neural pathway resulted in more bone resorption, decreased bone formation, trabecular bone loss, and decreased bone strength.[75] As a result, it is possible that the lack of calcitonin gene-related neuropeptide in unmyelinated neurons associated with FD or more generally the impaired nervous system plays a direct role in the bone loss of FD, but this hypothesis requires further investigation.

Important differences in bone are likely to exist for our mouse model and human FD. Nonetheless, our data indicate that the bone fragility of FD may be related to loss of bone quality as opposed to just bone mass. Further work is needed to better understand the origins of loss of bone quality in FD and the potential efficacy of therapeutic approaches. This mouse model provides a needed platform for undertaking these investigations.

Our study has several limitations. It has not been determined whether ELP1 protein is present in bone although it has been shown to be expressed in muscle.[78] In our model, *Elp1* is only deleted from neurons, and thus all the reported phenotypes are expected to be the consequence of the altered nervous system.[5–8] Next, our assessment of bone quality was not exhaustive. further analysis of bone matrix quality (e.g., collagen crosslinking, collagen-mineral interactions) would improve our understanding of why bone toughness is reduced in our FD mouse model. Finally, bone microarchitecture is not conventionally assessed from PMMA embedded specimens. However, from prior work in which bones were scanned in both unembedded and PMMA-embedded conditions, we do not expect that PMMA have influenced our reported measures.[68,79–84] We did not assess BMD from microCT, since these prior reports did not evaluate whether this measure differs with PMMA-embedding. Following our identification of multiscale loss of bone quality in this FD mouse model, future work would benefit from a larger sample size at several specific ages, characterization of fresh bone tissue microarchitecture and composition, and dynamic histomorphometry.

5.0 Conclusions

We demonstrate that deletion of Elp1 in the nervous system reduces multiscale bone quality. FD reduced whole bone toughness. This decrease in toughness was negatively correlated with a Raman spectroscopy biomarker for damage to altered collagen secondary structure, indicating that FD alters either collagen secondary structure or the propensity of the bone to damage during processing for tissue-scale studies. Microarchitecture was also modified with FD, but only for females. FD is a multisystemic disease where numerous factors, including altered nervous system, altered nutrition, kidney function, and movement may impact bone quality. While the specific causes of bone quality loss with FD are challenging to interrogate, further investigation of bone quality impairments produced by this model may lead to critical insights that assist in the prevention and management of frequent bone fractures experienced by this population.

Supplementary Material

Refer to Web version on PubMed Central for supplementary material.

Acknowledgments

This research was made possible by the Department of Mechanical & Industrial Engineering and the College of Engineering at the Montana State University. C.H. and H.F. were supported by NIH P20 GM103474. F.L. and M.M. were supported by NIH R01s NS086796 and DK117473. The content is solely the responsibility of the authors and does not necessarily represent the official views of the National Institutes of Health.

6.0 References

[1]. Riley CM, Day RL, Central autonomic dysfunction with defective lacrimation; report of five cases., Pediatrics. 3 (1949) 468–478. [PubMed: 18118947]

[2]. Slaugenhaupt SA, Blumenfeld A, Gill SP, Leyne M, Mull J, Cuajungco MP, Liebert CB, Chadwick B, Idelson M, Reznik L, Tissue-specific expression of a splicing mutation in the IKBKAP gene causes familial dysautonomia, Am. J. Hum. Genet 68 (2001) 598–605. [PubMed: 11179008]

[3]. Maayan C, Kaplan E, Shachar SH, Peleg O, Godfrey S, Incidence of familial dysautonomia in Israel 1977–1981, Clin. Genet 32 (1987) 106–108. [PubMed: 3652488]

[4]. Anderson SL, Coli R, Daly IW, Kichula EA, Rork MJ, Volpi SA, Ekstein J, Rubin BY, Familial dysautonomia is caused by mutations of the IKAP gene, Am. J. Hum. Genet 68 (2001) 753–758. [PubMed: 11179021]

[5]. Lefcort F, Mergy M, Ohlen SB, Ueki Y, George L, Animal and cellular models of familial dysautonomia, Clin. Auton. Res 27 (2017) 235–243. doi:10.1007/s10286-017-0438-2. [PubMed: 28667575]

[6]. Cuajungco MP, Leyne M, Mull J, Gill SP, Lu W, Zagzag D, Axelrod FB, Maayan C, Gusella JF, Slaugenhaupt SA, Tissue-specific reduction in splicing efficiency of IKBKAP due to the major mutation associated with familial dysautonomia, Am. J. Hum. Genet 72 (2003) 749–758. [PubMed: 12577200]

[7]. Boone N, Loriod B, Bergon A, Sbai O, Formisano-Tréziny C, Gabert J, Khrestchatisky M, Nguyen C, Féron F, Axelrod FB, Olfactory stem cells, a new cellular model for studying molecular mechanisms underlying familial dysautonomia, PLoS One. 5 (2010) e15590. [PubMed: 21187979]

[8]. Chaverra M, George L, Mergy M, Waller H, Kujawa K, Murnion C, Sharples E, Thorne J, Podgajny N, Grindeland A, The familial dysautonomia disease gene IKBKAP is required in the developing and adult mouse central nervous system, Dis. Model. Mech 10 (2017) 605–618. [PubMed: 28167615]

[9]. Saper CB, The central autonomic nervous system: conscious visceral perception and autonomic pattern generation, Annu. Rev. Neurosci 25 (2002) 433–469. doi:10.1146/annurev.neuro.25.032502.111311. [PubMed: 12052916]

[10]. Beissner F, Meissner K, Bär K-J, Napadow V, The autonomic brain: an activation likelihood estimation meta-analysis for central processing of autonomic function, J. Neurosci 33 (2013) 10503–10511. [PubMed: 23785162]

[11]. Norcliffe-Kaufmann L, Axelrod F, Kaufmann H, Afferent baroreflex failure in familial dysautonomia, Neurology. 75 (2010) 1904–1911. [PubMed: 21098405]

[12]. Grünebaum M, Radiological manifestations in familial dysautonomia., Am. J. Dis. Child 128 (1974) 176–178. doi:10.1001/archpedi.1974.02110270050010. [PubMed: 4854017]

[13]. Filler J, Smith AA, Stone S, Dancis J, Respiratory control in familial dysautonomia, J. Pediatr 66 (1965) 509–516. [PubMed: 14264309]

[14]. Laplaza FJ, Turajane T, Axelrod FB, Burke SW, Nonspinal orthopaedic problems in familial dysautonomia (Riley-Day syndrome), J. Pediatr. Orthop 21 (2001) 229–232. doi:10.1097/00004694-200103000-00019. [PubMed: 11242256]

[15]. Palma J-A, Norcliffe-Kaufmann L, Fuente-Mora C, Percival L, Mendoza-Santiesteban C, Kaufmann H, Current treatments in familial dysautonomia, Expert Opin. Pharmacother 15 (2014) 2653–2671. doi:10.1517/14656566.2014.970530. [PubMed: 25323828]

[16]. Hernandez CJ, Keaveny TM, A biomechanical perspective on bone quality, Bone. 39 (2006) 1173–1181. [PubMed: 16876493]

[17]. Boskey AL, Imbert L, Bone quality changes associated with aging and disease: a review, Ann. N. Y. Acad. Sci 1410 (2017) 93–106. doi:10.1111/nyas.13572. [PubMed: 29265417]

[18]. Maayan C, Bar-On E, Foldes AJ, Gesundheit B, Pollak RD, Bone mineral density and metabolism in familial dysautonomia, Osteoporos. Int 13 (2002) 429–433. doi:10.1007/s001980200050. [PubMed: 12086355]

[19]. Bar-On E, Floman Y, Sagiv S, Katz K, Pollak RD, Maayan C, Orthopaedic manifestations of familial dysautonomia : A review of one hundred and thirty-six patients, JBJS. 82 (2000) 1563.

[20]. Dietrich P, Dragatsis I, Familial dysautonomia: Mechanisms and models, Genet. Mol. Biol 39 (2016) 497–514. doi:10.1590/1678-4685-GMB-2015-0335. [PubMed: 27561110]

[21]. Kaplan L, Marguilies JY, Kadari A, Floman Y, Robin GC, Aspects of spinal deformity in familial dysautonomia (Riley-Day syndrome), Eur. Spine J 6 (1997) 33–38. [PubMed: 9093825]

[22]. Krausz Y, Maayan C, Faber J, Marciano R, Mogle P, Wynchank S, Scintigraphic evaluation of esophageal transit and gastric emptying in familial dysautonomia, Eur. J. Radiol 18 (1994) 52–56. [PubMed: 8168583]

[23]. Norcliffe-Kaufmann L, Axelrod FB, Kaufmann H, Developmental abnormalities, blood pressure variability and renal disease in Riley Day syndrome, J. Hum. Hypertens 27 (2013) 51–55. doi:10.1038/jhh.2011.107. [PubMed: 22129610]

[24]. Blumenfeld A, Slaugenhaupt SA, Liebert CB, Temper V, Maayan C, Gill S, Lucente DE, Idelson M, MacCormack K, Monahan MA, Precise genetic mapping and haplotype analysis of the familial dysautonomia gene on human chromosome 9q31, Am. J. Hum. Genet 64 (1999) 1110–1118. [PubMed: 10090896]

[25]. Ketteler M, Block GA, Evenepoel P, Fukagawa M, Herzog CA, McCann L, Moe SM, Shroff R, Tonelli MA, Toussaint ND, Vervloet MG, Leonard MB, Executive summary of the 2017 KDIGO Chronic Kidney Disease–Mineral and Bone Disorder (CKD-MBD) Guideline Update: what's changed and why it matters, Kidney Int. 92 (2017) 26–36. doi:10.1016/j.kint.2017.04.006. [PubMed: 28646995]

[26]. George L, Chaverra M, Wolfe L, Thorne J, Close-Davis M, Eibs A, Riojas V, Grindeland A, Orr M, Carlson GA, Familial dysautonomia model reveals Ikbkap deletion causes apoptosis of Pax3+ progenitors and peripheral neurons, Proc. Natl. Acad. Sci 110 (2013) 18698–18703. [PubMed: 24173031]

[27]. Ueki Y, Ramirez G, Salcedo E, Stabio ME, Lefcort F, Loss of Ikbkap causes slow, progressive retinal degeneration in a mouse model of familial dysautonomia, eNeuro. 3 (2016). doi:10.1523/ENEURO.0143-16.2016.

[28]. Morini E, Dietrich P, Salani M, Downs HM, Wojtkiewicz GR, Alli S, Brenner A, Nilbratt M, LeClair JW, Oaklander AL, Slaugenhaupt SA, Dragatsis I, Sensory and autonomic deficits in a new humanized mouse model of familial dysautonomia, Hum. Mol. Genet 25 (2015) 1116–1128. doi:10.1093/hmg/ddv634.

[29]. Dietrich P, Alli S, Shanmugasundaram R, Dragatsis I, IKAP expression levels modulate disease severity in a mouse model of familial dysautonomia, Hum. Mol. Genet 21 (2012) 5078–5090. doi:10.1093/hmg/dds354. [PubMed: 22922231]

[30]. Jackson MZ, Gruner KA, Qin C, Tourtellotte WG, A neuron autonomous role for the familial dysautonomia gene ELP1 in sympathetic and sensory target tissue innervation, Development. 141 (2014) 2452–2461. [PubMed: 24917501]

[31]. Chen Y-T, Hims MM, Shetty RS, Mull J, Liu L, Leyne M, Slaugenhaupt SA, Loss of mouse Ikbkap, a subunit of elongator, leads to transcriptional deficits and embryonic lethality that can be rescued by human IKBKAP, Mol. Cell. Biol 29 (2009) 736–744. [PubMed: 19015235]

[32]. Dietrich P, Yue J, Shuyu E, Dragatsis I, Deletion of exon 20 of the Familial Dysautonomia gene Ikbkap in mice causes developmental delay, cardiovascular defects, and early embryonic lethality, PLoS One. 6 (2011) e27015. [PubMed: 22046433]

[33]. Turner CH, Burr DB, Basic biomechanical measurements of bone: A tutorial, Bone. 14 (1993) 595–608. doi:10.1016/8756-3282(93)90081-K. [PubMed: 8274302]

[34]. Heveran CM, Ortega AM, Cureton A, Clark R, Livingston EW, Bateman TA, Levi M, King KB, Ferguson VL, Moderate chronic kidney disease impairs bone quality in C57Bl/6J mice, Bone. 86 (2016) 1–9. doi:10.1016/j.bone.2016.02.006. [PubMed: 26860048]

[35]. Bouxsein ML, Boyd SK, Christiansen BA, Guldberg RE, Jepsen KJ, Müller R, Guidelines for assessment of bone microstructure in rodents using micro-computed tomography, J. Bone Miner. Res 25 (2010) 1468–1486. doi:10.1002/jbmr.141. [PubMed: 20533309]

[36]. Heveran CM, Ortega AM, Cureton A, Clark R, Livingston EW, Bateman TA, Levi M, King KB, Ferguson VL, Moderate chronic kidney disease impairs bone quality in C57Bl/6J mice, Bone. 86 (2016) 1–9. doi:PMC4833654. [PubMed: 26860048]

[37]. Heveran CM, Schurman CA, Acevedo C, Livingston EW, Howe D, Schaible EG, Hunt HB, Rauff A, Donnelly E, Carpenter RD, Levi M, Lau AG, Bateman TA, Alliston T, King KB, Ferguson VL, Chronic kidney disease and aging differentially diminish bone material and microarchitecture in a, Bone. 127 (2019) 91–103. doi:10.1016/j.bone.2019.04.019. [PubMed: 31055118]

[38]. Ebenstein DM, Pruitt LA, Nanoindentation of biological tissues, Nano Today. 1 (2006) 26–33.

[39]. Oliver WC, Pharr GM, An improved technique for determining hardness and elastic modulus using load and displacement sensing indentation experiments, J. Mater. Res 7 (1992) 1564–1583.

[40]. Ferguson VL, Bushby AJ, Boyde A, Nanonmechanical properties and mineral concentration in articular calcified cartilage and subchondral bone, J. Anat 203 (2003) 191–202. doi:10.1046/j.1469-7580.2003.00193.x. [PubMed: 12924819]

[41]. Unal M, Jung H, Akkus O, Novel Raman Spectroscopic Biomarkers Indicate That Postyield Damage Denatures Bone's Collagen, J. Bone Miner. Res 31 (2016) 1015–1025. doi:10.1002/jbmr.2768. [PubMed: 26678707]

[42]. Ferguson VL, Ayers RA, Bateman TA, Simske SJ, Bone development and age-related bone loss in male C57BL/6J mice, Bone. 33 (2003) 387–398. doi:10.1016/S8756-3282(03)00199-6. [PubMed: 13678781]

[43]. Halloran BP, Ferguson VL, Simske SJ, Burghardt A, Venton LL, Majumdar S, Changes in bone structure and mass with advancing age in the male C57BL/6J mouse, J. Bone Miner. Res 17 (2002) 1044–1050. doi:10.1359/jbmr.2002.17.6.1044. [PubMed: 12054159]

[44]. De Winter JFC, Dodou D, Five-point likert items: t test versus Mann-Whitney-Wilcoxon (Addendum added October 2012), Pract. Assessment, Res. Eval 15 (2010) 11.

[45]. Fay MP, Proschan MA, Wilcoxon-Mann-Whitney or t-test? On assumptions for hypothesis tests and multiple interpretations of decision rules, Stat. Surv 4 (2010) 1–39. doi:10.1214/09-SS051. [PubMed: 20414472]

[46]. Sullivan GM, Artino AR Jr, Analyzing and interpreting data from likert-type scales, J. Grad. Med. Educ 5 (2013) 541–542. doi:10.4300/JGME-5-4-18. [PubMed: 24454995]

[47]. Glatt V, Canalis E, Stadmeyer L, Bouxsein ML, Age-related changes in trabecular architecture differ in female and male C57BL/6J mice, J. Bone Miner. Res 22 (2007) 1197–1207. doi:10.1359/jbmr.070507. [PubMed: 17488199]

[48]. Somerville JM, Aspden RM, Armour KE, Armour KJ, Reid DM, Growth of C57Bl/6 Mice and the Material and Mechanical Properties of Cortical Bone from the Tibia, Calcif. Tissue Int 74 (2004) 469–475. doi:10.1007/s00223-003-0101-x. [PubMed: 14961209]

[49]. Ab-Lazid R, Perilli E, Ryan MK, Costi JJ, Reynolds KJ, Does cancellous screw insertion torque depend on bone mineral density and/or microarchitecture?, J. Biomech 47 (2014) 347–353. doi:10.1016/j.jbiomech.2013.11.030. [PubMed: 24360200]

[50]. Perilli E, Briggs AM, Kantor S, Codrington J, Wark JD, Parkinson IH, Fazzalari NL, Failure strength of human vertebrae: Prediction using bone mineral density measured by DXA and bone volume by micro-CT, Bone. 50 (2012) 1416–1425. doi:10.1016/j.bone.2012.03.002. [PubMed: 22430313]

[51]. Karim L, Vashishth D, Role of trabecular microarchitecture in the formation, accumulation, and morphology of microdamage in human cancellous bone, J. Orthop. Res 29 (2011) 1739–1744. doi:10.1002/jor.21448. [PubMed: 21538510]

[52]. Bahar H, Gallacher K, Downall J, Nelson CA, Shomali M, Hattersley G, Six Weeks of Daily Abaloparatide Treatment Increased Vertebral and Femoral Bone Mineral Density, Microarchitecture and Strength in Ovariectomized Osteopenic Rats, Calcif. Tissue Int 99 (2016) 489–499. doi:10.1007/s00223-016-0171-1. [PubMed: 27395059]

[53]. Eddy DM, Johnston J, Cummings SR, Dawson-Hughes B, Lindsay R, Melton LJ, Slemenda CW, Osteoporosis: review of the evidence for prevention, diagnosis, and treatment and cost-effectiveness analysis. Status report, Osteoporos. Int 8 (1998) I–S82.

[54]. Norcliffe-Kaufmann L, Slaugenhaupt SA, Kaufmann H, Familial dysautonomia: History, genotype, phenotype and translational research, Prog. Neurobiol 152 (2017) 131–148. doi:10.1016/j.pneurobio.2016.06.003. [PubMed: 27317387]

[55]. Zeltner N, Fattahi F, Dubois NC, Saurat N, Lafaille F, Shang L, Zimmer B, Tchieu J, Soliman MA, Lee G, Capturing the biology of disease severity in a PSC-based model of familial dysautonomia, Nat. Med 22 (2016) 1421. [PubMed: 27841875]

[56]. Creecy A, Uppuganti S, Unal M, Bunn RC, Voziyan P, Nyman JS, Low bone toughness in the TallyHO model of juvenile type 2 diabetes does not worsen with age, Bone. 110 (2018) 204–214. [PubMed: 29438824]

[57]. Unal M, Uppuganti S, Timur S, Mahadevan-Jansen A, Akkus O, Nyman JS, Assessing matrix quality by Raman spectroscopy helps predict fracture toughness of human cortical bone, Sci. Rep 9 (2019) 1–13. doi:10.1038/s41598-019-43542-7. [PubMed: 30626917]

[58]. Creecy A, Uppuganti S, Girard MR, Schlunk SG, Amah C, Granke M, Unal M, Does MD, Nyman JS, The age-related decrease in material properties of BALB/c mouse long bones involves alterations to the extracellular matrix, Bone. 130 (2020) 115126. [PubMed: 31678497]

[59]. Hunt HB, Pearl JC, Diaz DR, King KB, Donnelly E, Bone tissue collagen maturity and mineral content increase with sustained hyperglycemia in the KK-Ay murine model of type 2 diabetes, J. Bone Miner. Res 33 (2018) 921–929. [PubMed: 29281127]

[60]. Saito M, Fujii K, Mori Y, Marumo K, Role of collagen enzymatic and glycation induced cross-links as a determinant of bone quality in spontaneously diabetic WBN/Kob rats, Osteoporos. Int 17 (2006) 1514–1523. [PubMed: 16770520]

[61]. Paschalis EP, Shane E, Lyritis G, Skarantavos G, Mendelsohn R, Boskey AL, Bone fragility and collagen cross-links, J. Bone Miner. Res 19 (2004) 2000–2004. [PubMed: 15537443]

[62]. Morgan S, Poundarik AA, Vashishth D, Do non-collagenous proteins affect skeletal mechanical properties?, Calcif. Tissue Int 97 (2015) 281–291. [PubMed: 26048282]

[63]. Nikel O, Laurencin D, McCallum SA, Gundberg CM, Vashishth D, NMR investigation of the role of osteocalcin and osteopontin at the organic–inorganic interface in bone, Langmuir. 29 (2013) 13873–13882. [PubMed: 24128197]

[64]. Bar-Shai A, Maayan C, Vromen A, Udassin R, Nissan A, Freund HR, Hanani M, Decreased density of ganglia and neurons in the myenteric plexus of familial dysautonomia patients, J. Neurol. Sci 220 (2004) 89–94. [PubMed: 15140612]

[65]. Axelrod FB, Familial dysautonomia and other congenital sensory and autonomic neuropathies, Cell. Mol. Biol. Neuronal Dev, Springer, 1984: p. 331–340.

[66]. Palma J-A, Kuafmann L, Fuente C, Percival L, Mendoza C, Kaufmann H, Current treatments in familial dysautonomia, J. Invest. Dermatol 15 (2014) 2653–2671. doi:10.1038/jid.2014.371.

[67]. Portnoy S, Maayan C, Tsenter J, Ofran Y, Goldman V, Hiller N, Karniel N, Schwartz I, Characteristics of ataxic gait in familial dysautonomia patients, PLoS One. 13 (2018) 1–14. doi:10.1371/journal.pone.0196599.

[68]. Newman CL, Creecy A, Granke M, Nyman JS, Tian N, Hammond MA, Wallace JM, Brown DM, Chen N, Moe SM, Allen MR, Raloxifene improves skeletal properties in an animal model of cystic chronic kidney disease, Kidney Int. 89 (2016) 95–104. doi:10.1038/ki.2015.315. [PubMed: 26489025]

[69]. Iwasaki Y, Kazama JJ, Yamato H, Matsugaki A, Nakano T, Fukagawa M, Altered material properties are responsible for bone fragility in rats with chronic kidney injury, Bone. 81 (2015) 247–254. doi:10.1016/j.bone.2015.07.015. [PubMed: 26187196]

[70]. Iwasaki Y, Kazama JJ, Yamato H, Fukagawa M, Changes in chemical composition of cortical bone associated with bone fragility in rat model with chronic kidney disease, Bone. 48 (2011) 1260–1267. [PubMed: 21397740]

[71]. Malluche HH, Porter DS, Monier-Faugere M-C, Mawad H, Pienkowski D, Differences in bone quality in low- and high-turnover renal osteodystrophy, J. Am. Soc. Nephrol 23 (2012) 525–532. doi:10.1681/ASN.2010121253. [PubMed: 22193385]

[72]. Mach DB, Rogers SD, Sabino MC, Luger NM, Schwei MJ, Pomonis JD, Keyser CP, Clohisy DR, Adams DJ, O'Leary P, Mantyh PW, Origins of skeletal pain: sensory and sympathetic innervation of the mouse femur., Neuroscience. 113 (2002) 155–166. doi:10.1016/s0306-4522(02)00165-3. [PubMed: 12123694]

[73]. Bjurholm A, Kreicbergs A, Brodin E, Schultzberg M, Substance P- and CGRP-immunoreactive nerves in bone., Peptides. 9 (1988) 165–171. doi:10.1016/0196-9781(88)90023-x. [PubMed: 2452430]

[74]. Elefteriou F, Regulation of bone remodeling by the central and peripheral nervous system, Arch. Biochem. Biophys 473 (2008) 231–236. doi:10.1016/j.abb.2008.03.016. [PubMed: 18410742]

[75]. Offley SC, Guo TZ, Wei T, Clark JD, Vogel H, Lindsey DP, Jacobs CR, Yao W, Lane NE, Kingery WS, Capsaicin-sensitive sensory neurons contribute to the maintenance of trabecular bone integrity, J. Bone Miner. Res 20 (2005) 257–267. doi:10.1359/JBMR.041108. [PubMed: 15647820]

[76]. Maayan C, Becker Y, Gesundheit B, Girgis SI, Calcitonin gene-related peptide in familial dysautonomia, Neuropeptides. 35 (2001) 189–195. doi:10.1054/npep.2001.0863. [PubMed: 11884210]

[77]. Pearson J, Dancis J, Axelrod F, Grover N, The sural nerve in familial dysautonomia., J. Neuropathol. Exp. Neurol 34 (1975) 413–424. doi:10.1097/00005072-197509000-00004. [PubMed: 1176995]

[78]. Mezey É, Parmalee A, Szalayova I, Gill SP, Cuajungco MP, Leyne M, Slaugenhaupt SA, Brownstein MJ, Of splice and men: what does the distribution of IKAP mRNA in the rat tell us about the pathogenesis of familial dysautonomia?, Brain Res. 983 (2003) 209–214. [PubMed: 12914982]

[79]. Perilli E, Baruffaldi F, Visentin M, Bordini B, Traina F, Cappello A, Viceconti M, MicroCT examination of human bone specimens: Effects of polymethylmethacrylate embedding on structural parameters, J. Microsc 225 (2007) 192–200. doi:10.1111/j.1365-2818.2007.01731.x. [PubMed: 17359254]

[80]. Particelli F, Mecozzi L, Beraudi A, Montesi M, Baruffaldi F, Viceconti M, A comparison between micro-CT and histology for the evaluation of cortical bone: Effect of polymethylmethacrylate embedding on structural parameters, J. Microsc 245 (2012) 302–310. doi:10.1111/j.1365-2818.2011.03573.x. [PubMed: 22106931]

[81]. Drews S, Beckmann F, Herzen J, Brunke O, Salmon P, Friess S, Laib A, Koller B, Hemberger T, Müller-Gerbl M, Müller B, Comparative micro computed tomography study of a vertebral body, Dev. X-Ray Tomogr. VI 7078 (2008) 70780C. doi:10.1117/12.793815.

[82]. Thomsen JS, Laib A, Koller B, Prohaska S, Mosekilde L, Gowin W, Stereological measures of trabecular bone structure: comparison of 3D micro computed tomography with 2D histological sections in human proximal tibial bone biopsies, J. Microsc 218 (2005) 171–179. [PubMed: 15857378]

[83]. Kuhn JL, Goldstein SA, Feldkamp LA, Goulet RW, Jesion G, Evaluation of a microcomputed tomography system to study trabecular bone structure, J. Orthop. Res 8 (1990) 833–842. doi:10.1002/jor.1100080608. [PubMed: 2213340]

[84]. Ito M, Nakamura T, Matsumoto T, Tsurusaki K, Hayashi K, Analysis of trabecular microarchitecture of human iliac bone using microcomputed tomography in patients with hip arthrosis with or without vertebral fracture, Bone. 23 (1998) 163–169. doi:10.1016/S8756-3282(98)00083-0. [PubMed: 9701476]

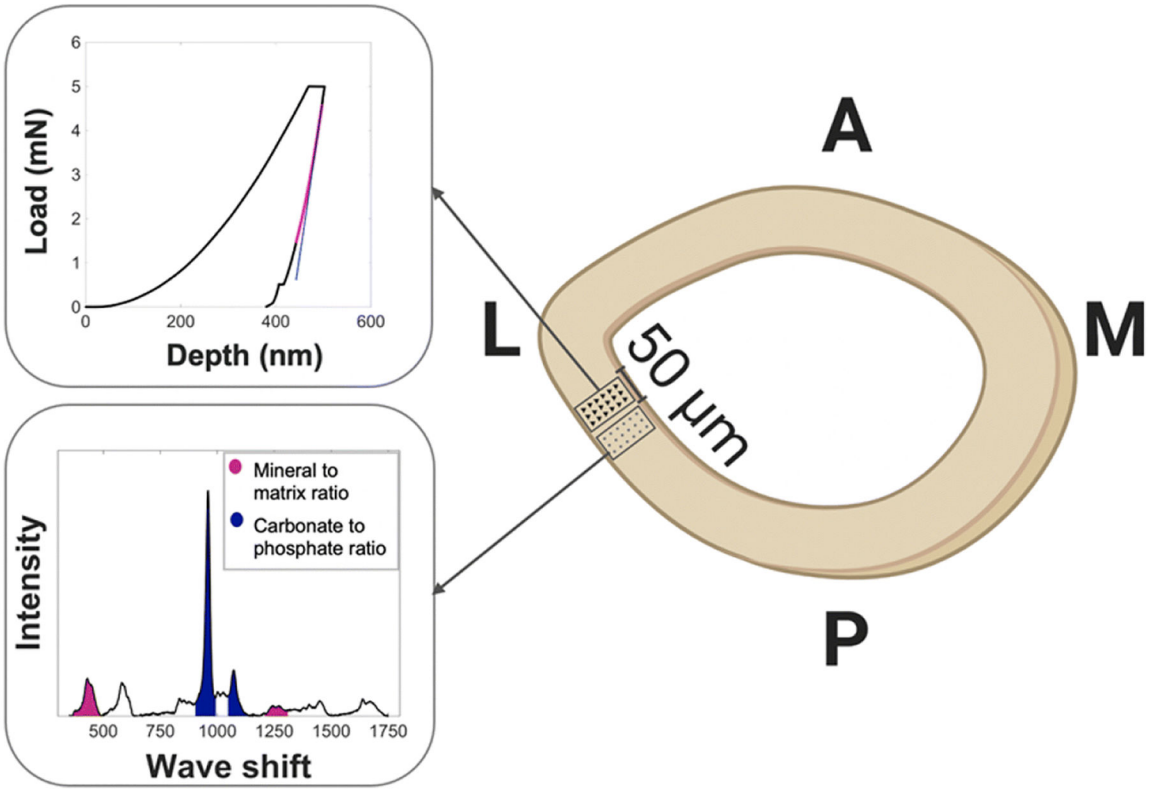

Figure 1.

Tissue-scale bone material analyses using nanoindentation and Raman spectroscopy. Arrays for each analysis spanned the cortical thickness in the lateral-posterior quadrant from the mid-diaphysis of the femurs.

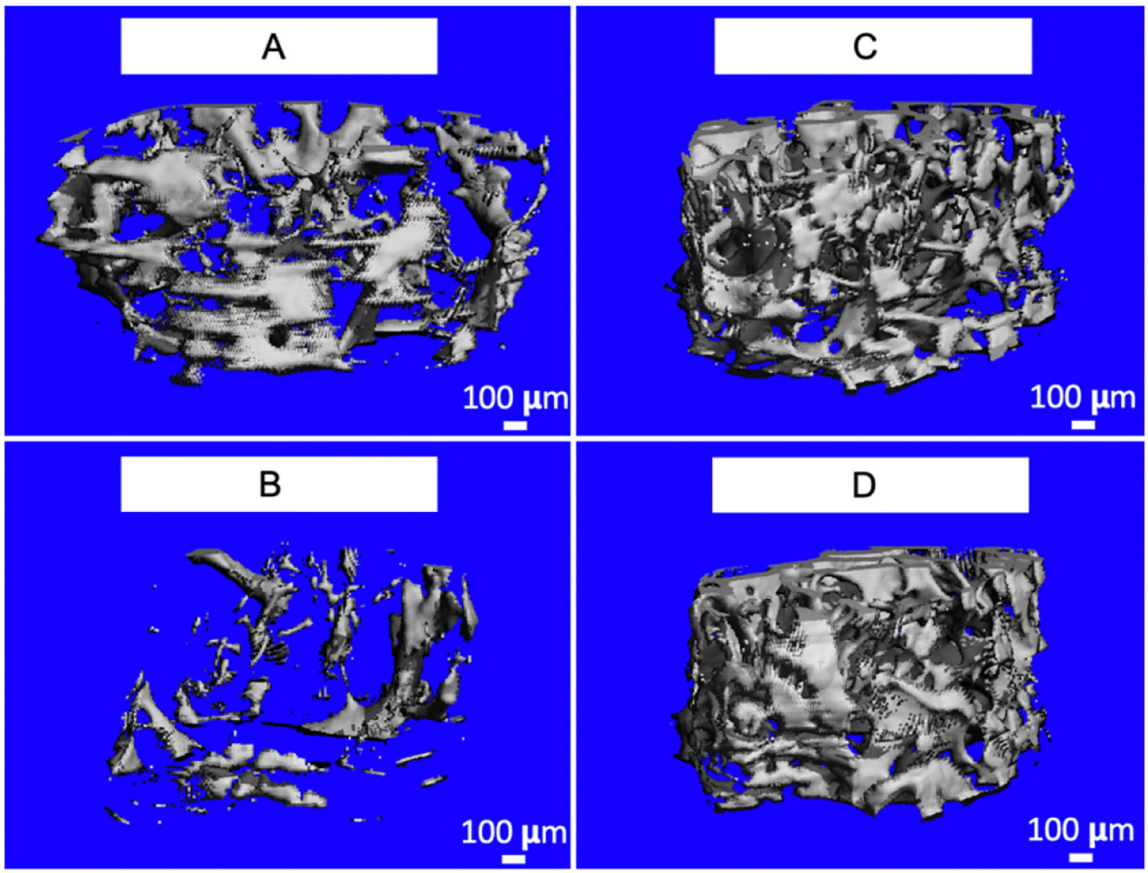

Figure 2.

Representative microCT images for A) Control female, B) FD female, C) Control male, and D) FD male, showing the trabecular differences from FD between sexes for representative data.

Table 1:

Disease severity and mouse size.

Measure	Female		Male	
	Control n = 5	**FD n = 7**	**Control n = 6**	**FD n = 4**
Age (month) Sex: NS FD: NS Sex x FD: NS	9.5 ± 0.0	9.8 ± 0.1	9.2 ± 0.2	8.8 ± 0.1
Body mass (g) ***Sex*:** p = 0.002 ***FD*:** p = 0.015 ***Sex x FD*:** p = 0.031	27.2 ± 2.0	26.7 ± 2.6	34.5 ± 4.1	28.2 ± 1.5 *p = 0.003, −18.3%
Femur length (mm) ***Sex*:** p = 0.009 FD: NS Sex x FD: NS	14.7 ± 0.3	15.1 ± 0.5	14.4 ± 0.3	14.6 ± 0.3
Disease severity ***Sex*:** p = 0.014	0.0 ± 0.0	3.9 ± 1.6	0.0 ± 0.0	6.3 ± 1.0

Data are presented as mean ± standard deviation.

* = significant difference between male control and FD mice.

Table 2:

Trabecular microarchitecture and cortical geometry

Measure	Female		Male	
	Control n = 5	**FD n = 7**	**Control n = 6**	**FD n = 4**
Trabecular microarchitecture				
BV ***Sex*:** p < 0.001 ***FD*:** p = 0.011 ***Sex x FD*:** p = 0.005	0.13 ± 0.04	0.05 ± 0.03 $^{\#}$p < 0.001; −57.8%	0.39 ± 0.10	0.41 ± 0.08
TV Sex: NS ***FD*:** p = 0.018 Sex x FD: NS	2.61 ± 0.15	2.45 ± 0.19	2.71 ± 0.14	2.52 ± 0.08
BV/TV ***Sex*:** p < 0.001 ***FD*:** p = 0.031 ***Sex x FD*:** p = 0.005	0.05 ± 0.02	00.02 ± 0.01 $^{\#}$p =0.001; −55.4%	0.14 ± 0.04	0.16 ± 0.03
Conn.D ***Sex*:** p < 0.001 FD: NS ***Sex x FD*:** p = 0.001	31.10 ± 27.50	6.77 ± 11.60 $^{\#}$p = 0.006; −78.2%	77.70 ± 28.20	136.09 ± 12.46 *p = 0.015; +75.2%
SMI ***Sex*:** p < 0.001 FD: NS ***Sex x FD*:** p = 0.006	2.30 ± 0.39	3.04 ± 0.39 $^{\#}$p = 0.002; +32.2%	1.67 ± 0.34	1.43 ± 0.30
Tb.N ***Sex*:** p < 0.001 FD: NS Sex x FD: NS	1.78 ± 0.63	1.93 ± 0.22	3.46 ± 0.54	3.85 ± 0.39
Tb.Th Sex: NS ***FD*:** p = 0.020 Sex x FD: NS	0.05 ± 0.01	0.04 ± 0.01	0.06 ± 0.01	0.05 ± 0.00
Tb.Sp ***Sex*:** p < 0.001 FD: NS Sex x FD: NS	0.65 ± 0.27	0.53 ± 0.06	0.28 ± 0.06	0.26 ± 0.03
Cortical microarchitecture				
I_{min} (mm^4) ***Sex*:** p = 0.006	0.134 ± 0.009	0.130 ± 0.028	0.181 ± 0.035	0.164 ± 0.039

Measure	**Female**		**Male**	
	Control n = 5	**FD n = 7**	**Control n = 6**	**FD n = 4**
FD: NS Sex x FD: NS				
Ct. Th (mm) Sex: NS FD: NS Sex x FD: NS	0.221 ± 0.018	0.224 ± 0.022	0.216 ± 0.049	0.226 ± 0.031
Ct. Ar (mm ^{2}) ***Sex*:** p = 0.007 FD: NS Sex x FD: NS	0.831 ± 0.047	0.825 ± 0.084	0.970 ± 0.116	0.956 ± 0.154

Data are presented as mean ± standard deviation.

 # = significant difference compared with female control mice,

** =* significant difference compared with male control mice.

Table 3:

Whole-bone material and mechanical properties from three-point flexural testing

Measure	Female		Male	
	Control n = 5	**FD n = 7**	**Control n = 6**	**FD n = 4**
Stiffness (N/mm) ***Sex*:** p = 0.020 FD: NS Sex x FD: NS	94.1 ± 13.8	81.2 ± 11.6	102.4 ± 12.4	101.1 ± 13.8
Maximum force (N) ***Sex*:** p = 0.016 FD: NS Sex x FD: NS	18.7 ± 1.4	18.0 ± 2.1	21.2 ± 2.5	20.4 ± 2.3
Work to Fracture (mJ) Sex: NS ***FD*:** p = 0.004 Sex x FD: NS	7.7 ± 1.8	6.6 ± 2.0	10.3 ± 2.5	5.6 ± 1.6
Modulus (GPa) Sex: NS FD: NS Sex x FD: NS	7.6 ± 1.4	7.1 ± 1.8	6.6 ± 1.7	6.9 ± 1.7
Maximum strength (MPa) Sex: NS FD: NS Sex x FD: NS	185.0 ± 19.0	174.8 ± 24.5	161.8 ± 16.7	172.2 ± 23.2
Toughness (MJ/m ^{3}) Sex: NS ***FD*:** p = 0.001 Sex x FD: NS	8.3 ± 1.1	6.1 ± 2.4	8.8 ± 1.8	4.2 ± 1.9

Data are presented as mean ± standard deviation.

Table 4:

Bone tissue material properties from nanoindentation, Raman spectroscopy, and DXA

Measure	Female		Male	
	Control n = 5	**FD n = 7**	**Control n = 6**	**FD n = 4**
Mean E_i (GPa) Sex: NS ***FD*:** p= 0.041 Sex x FD: NS	31.66 ± 1.63	29.95 ± 1.79	30.32 ± 1.99	28.50 ± 1.12
sd E_i (GPa) Sex: NS FD: NS Sex x FD: NS	3.39 ± 0.37	3.50 ± 0.80	3.32 ± 0.25	2.89 ± 0.80
Mean mineral:matrix Sex: NS FD: NS Sex x FD: NS	5.16 ± 0.57	4.95 ± 0.20	4.56 ± 0.67	4.63 ± 0.77
sd mineral:matrix Sex: NS FD: NS Sex x FD: NS	0.84 ± 0.16	0.89 ± 0.31	0.80 ± 0.51	0.99 ± 0.54
Mean carbonate:phosphate Sex: NS FD: NS Sex x FD: NS	0.09 ± 0.01	0.09 ± 0.00	0.10 ± 0.01	0.09 ± 0. 01
sd carbonate:phosphate Sex: NS FD: NS Sex x FD: NS	0.007 ± 0.002	0.008 ± 0.001	0.006 ± 0.002	0.007 ± 0.001
Mean crystallinity ***Sex*:** p = 0.057 FD: NS Sex x FD: NS	0.050 ± 0.001	0.051 ± 0.001	0.053 ± 0.003	0.053 ± 0.005
sd crystallinity Sex: NS FD: NS Sex x FD: NS	0.001 ± 0.000	0.001 ± 0.000	0.001 ± 0.000	0.001 ± 0.000
Mean I1670:I1640 ***Sex*:** p = 0.005	0.97 ± 0.19	0.97 ± 0.15	1.02 ± 0.08	1.29 ± 0.10

Measure	Female		Male	
	Control n = 5	**FD n = 7**	**Control n = 6**	**FD n = 4**
***FD*:** p = 0.031 ***Sex x FD*:** p = 0.032				*p = 0.006; +27.3%
Mean I1670:I1690 ***Sex*:** p = 0.002 ***FD*:** p = 0.030 Sex x FD: NS	1.36 ± 0.09	1.40 ± 0.11	1.46 ± 0.08	1.62 ± 0.11
Mean I1670:I1610 Sex: NS FD: NS Sex x FD: NS	3.03 ± 0.18	3.01 ± 0.29	3.00 ± 0.22	2.86 ± 0.26
DXA BMD (mg/cm2) ***Sex*:** p = 0.006 FD: NS Sex x FD: NS	62.74 ± 3.56 (n=4)	73.11 ± 9.21	78.18 ± 6.84	86.18 ± 12.60

Data are presented as mean ± standard deviation.

 # = significant difference compared with female control mice,

** =* significant difference compared with male control mice.